Damage assessment of linear structures by a static approach, II: Numerical simulation studies

Shih-Shong Tseng†

Department of Civil Engineering, National Kaohsiung Institute of Technology, 415 Cheng Kung Road, Kaohsiung 807, Taiwan, R.O.C.

Abstract. To confirm the theory and static defect energy (SDE) equations proposed in the first part, extensive numerical simulation studies are performed in this portion. Stiffness method is applied to calculate the components of the stresses and strains from which the energy components and finally, the SDE are obtained. Examples are designed to cover almost all kinds of possibilities. Variables include structural type, material, cross-section, support constraint, loading type, magnitude and position. The SDE diagram is unique in the way of presenting damage information: two different energy constants are separated by a sharp vertical drop right at the damage location. Simulation results are successfully implemented for both methods in all the cases.

Key words: damage assessment; static defect energy; stiffness method.

1. Introduction

Static approach for global damage detection can be considered as the result of evolution from dynamic methods. It is strongly focused only in recent years. Hajela and Soeiro (1990) used static deflections and vibration modes for system identification. Sanayei and Onipede (1991) used static test data to identify changes in structural element stiffness. Banan *et al.* (1994a, b) also processed parameter estimation from static response. Static approach is taken to avoid the noise-induced uncertainties in dealing with dynamic signals.

In the first part of the research, equations of the static defect energy have been derived. The energy gap provides a simple and yet strong physical concept with damage information. In this part, we shall apply the stiffness method to obtain the stresses and strains needed in the equations. Damage locations are not known in real practice. However, we have to assume one or more on an element in order to obtain the static responses for simulation. By taking static response data at two stages, P energy can be calculated and the SDE diagram can be established.

2. Numerical simulation method

Consider a plane beam/frame element shown in Fig. 1, the basic force matrix $\boldsymbol{B}$ consists of two bending moments M_i, M_j and an axial force N. The basic deformation matrix Δ consists of two rotations θ_i, θ_j and a linear elongation δ. Matrices f' and f are element end force vectors in the local
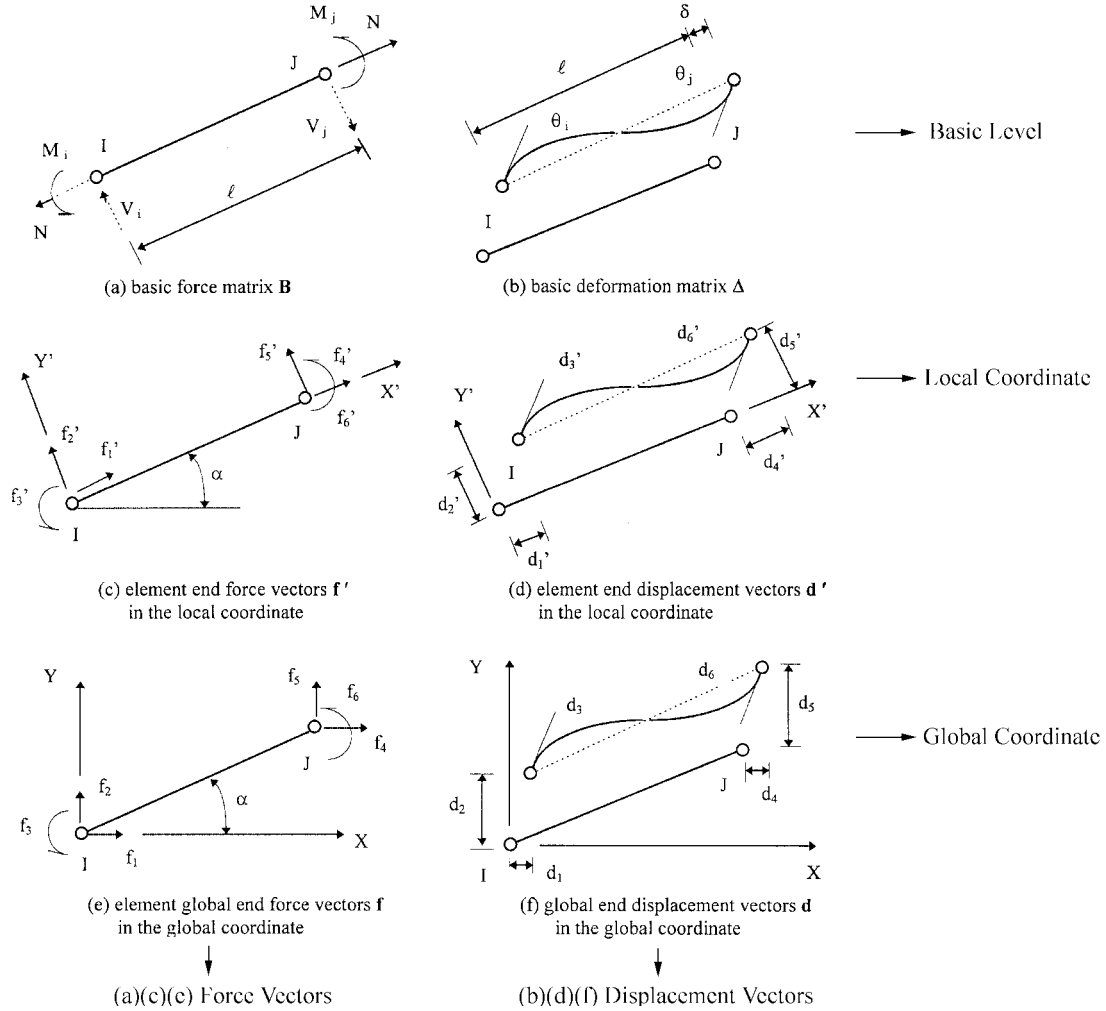
---

† Associate Professor

Fig. 1 Force and deformation components of a plane beam/frame element

and global coordinate while d' and d are element end displacement vectors also in the local and global coordinate, respectively. All theses matrices are 6×1 in their orders. Letters in bold-face represent the notation of matrices. The relationship between basic force and deformation vectors can be established as

$$B = \bar{k}\Delta \qquad (1)$$

where

$$\bar{k} = \frac{2EI}{l}\begin{bmatrix} 2 & 1 & 0 \\ 1 & 2 & 0 \\ 0 & 0 & A/2I \end{bmatrix} \qquad (2)$$

Applying the force equilibrium between Figs. 1(a) and (c), we have

$$f' = HB \qquad (3)$$

where H is the matrix of the coefficients of the basic forces.

$$H=\begin{bmatrix} 0 & 0 & -1 \\ 1/l & 1/l & 0 \\ 1 & 0 & 0 \\ 0 & 0 & 1 \\ -1/l & -1/l & 0 \\ 0 & 1 & 0 \end{bmatrix} \tag{4}$$

From the geometry of deformation relationship between Figs. 1(b) and (d), compatibility equation can be found.

$$\Delta = H^T d' \tag{5}$$

Superscript T indicates transpose of a matrix. Substituting Eqs. (5) and (1) into Eq. (3), yields the constitutive equation in the local coordinate

$$f' = k'd' \tag{6}$$

where

$$k'=H\bar{k}H^T \tag{7}$$

For a member in the global coordinate with an orientation angle α, the end force matrix f can be calculated through coordinate transformation.

$$f = Rf' \tag{8}$$

where R is the rotation matrix. Since d and f are an energy conjugate pair, the following equation can be found directly by using the contra-gradient law.

$$d'=R^T d \tag{9}$$

Substitute Eq. (9) and (6) into Eq. (8), the elemental stiffness equation in the global coordinate yields

$$f = kd \tag{10}$$

where

$$k=\frac{2EI}{l}\begin{bmatrix} \left(\frac{A}{2I}\right)c^2 + \left(\frac{6}{l^2}\right)s^2 \\ \left(\frac{A}{2I} - \frac{6}{l^2}\right)sc & \left(\frac{A}{2I}\right)s^2 + \left(\frac{6}{l^2}\right)c^2 & & \text{symmetric} \\ -\frac{3}{l}s & \frac{3}{l}c & 2 \\ -\left(\frac{A}{2I}\right)c^2 - \left(\frac{6}{l^2}\right)s^2 & -\left(\frac{A}{2I} - \frac{6}{l^2}\right)sc & \frac{3}{l}s & \left(\frac{A}{2I}\right)c^2 + \left(\frac{6}{l^2}\right)s^2 \\ -\left(\frac{A}{2I} - \frac{6}{l^2}\right)sc & -\left(\frac{A}{2I}\right)s^2 - \left(\frac{6}{l^2}\right)c^2 & -\frac{3}{l}c & \left(\frac{A}{2I} - \frac{6}{l^2}\right)sc & \left(\frac{A}{2I}\right)s^2 + \left(\frac{6}{l^2}\right)c^2 \\ -\frac{3}{l}s & \frac{3}{l}c & 1 & \frac{3}{l}s & -\frac{3}{l}c & 2 \end{bmatrix} \tag{11}$$

A, I, and l are cross-section, moment of inertia, and the length of the element, respectively, while $c = \cos\alpha$ and $s = \sin\alpha$ for simplification. Once the stiffness matrices for all the elements were obtained, a location matrix can be established to connect the local and global degree of freedom for each element. Let N_e represent total number of elements. The unconstrained structural stiffness matrix K, can be calculated by direct addition of the element stiffness matrices.

$$K = \sum_{n=1}^{N_e} k^{(e)} \tag{12}$$

Assume D_u and F_s are deformation and force matrices corresponding to the unknown quantities, and D_s and F_u are deformation and force matrices corresponding to the specified quantities of the global DOF. By matrix partition, structural stiffness equation gives

$$\begin{Bmatrix} F_u \\ F_s \end{Bmatrix} = \begin{bmatrix} K_{uu} & K_{us} \\ K_{su} & K_{ss} \end{bmatrix} \begin{Bmatrix} D_u \\ D_s \end{Bmatrix} \tag{13}$$

K_{uu}, K_{us}, K_{su} and K_{ss} are subdivided matrices of K. Thus, the free DOF of the nodes, D_u, and the unknown force quantities, F_s, can be obtained in sequence. Apply Eq. (9) to each member, d' can be calculated. Back substitute local end displacement vectors into the compatibility equation, θ_i, θ_j and δ are found. By using Eq. (1), the basic force vectors M_i, M_j and axial force N are calculated. Shear forces on the node equal

$$V_i = V_j = \frac{1}{l}(M_i + M_j) \tag{14}$$

Curvature κ at node i can be derived simply by dividing bending moment by its flexural rigidity, i.e.,

$$\kappa_i = -\frac{M_i}{EI} \tag{15}$$

Shear strain γ can be calculated from the shear force V

$$\gamma_i = \frac{V_i}{\gamma_c GA} \tag{16}$$

where GA is the shearing rigidity, and γ_c is the shear correction factor that is used to modify the non-uniform shear stress distribution across its cross-section. All terms needed for P energy at each node are now, obtained. If stress and strain quantities of an element are desired, they can be calculated simply by taking average from its two ends.

Energy components for bending, shearing and axial elongation effects can be calculated as:

$$W(\kappa) = \frac{1}{2}EI\kappa^2, \quad W(\gamma) = \frac{1}{2}GA\gamma^2, \quad W(\varepsilon) = \frac{1}{2}EA\varepsilon^2 \tag{17}$$

For damaged structures, the only change in the input FEM model is the specified defective element. Young's modulus is deducted by a certain percentage to modify different damage severity in the FEM model. For example, 0.9E is used on element 13th to represent a 10% damage on that element, while the rest of material constants, such as, area, moment of inertia, and shear modulus remain unchanged. Damage index, Di, can be defined as the ratio of the damaged area to the original area as shown in Fig. 2.
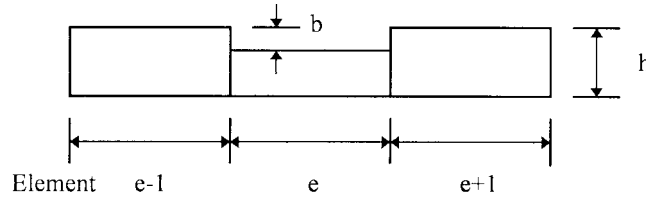
Fig. 2 The damage index model

$$Di = \frac{A_d}{A} = \frac{b}{h} \tag{18}$$

It is not necessarily related to any type of damage of the fracture mechanics. Therefore, a 10% damage can be expressed as $Di = 0.1$. This assumption is consistent with others, for instance, Gudmudson (1982, 1983) and Christides and Barr (1984, 1986).

In the subsequent calculation for P energy, intact E value will be used throughout each element including the infected damage ones since damage locations are not known in the real situation. Following the steps outlined in part I of this papers, the final results of SDE for both implementation methods can be obtained.

3. Numerical examples

The objective of doing numerical study is to verify the proposed parameter by exhausting every possibility. We choose hot rolled steel, aluminum, and light gage cold-form steel as the materials; box, bar, channel, and wide flange as the cross-sections; continuous, cantilever, and simply support as the structural constraints; concentrated and uniformly distributed load as the loading types. Therefore, almost all kinds of possibilities are included in this study. The simulated cases are listed in Table 1. Since the axial elongation is very small for the beam element, it can be neglected in the calculation.

Case 1. A continuous steel bridge-1

A two-span continuous beam shown in Fig. 3 is adopted to simulate a highway bridge. The main

Table 1 The simulated damage cases

Case No.	Structure	Cross section	Material	Damage location	Loading		
					type*	magnitude	position**
1	continuous beam	box	ASTM A242 steel	E13	c	+20 KN	N27
2	continuous beam	box	ASTM A242 steel	E13	c	+20 KN	N32
3	continuous beam	box	aluminum	E13	u	-500 N/m	E21 - E40
4	cantilever beam	circular bar	hot rolled steel	E15	c	-500 N	N1
5	simple beam	2 channels back to back	light gage cold-form steel	E30	c	-2.94 KN	N60
6	rigid frame	wide flange	ASTM A36 steel	E5, E12, E27, E43	u	+510 N/m	E51 - E70

*loading type: c - concentrated load, u - uniformly distributed load
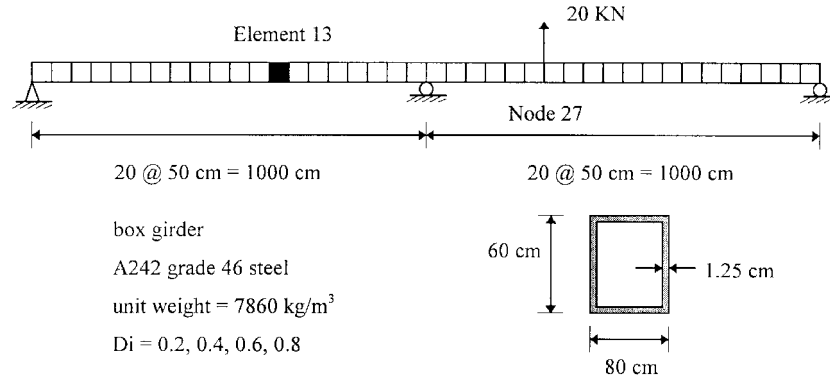**loading position: N - node number, E - element number

Fig. 3 Continuous steel bridge for case 1, the dimensions, properties, and finite element model

girder has a box cross section which is made of four ASTM A242 steel plates welded together. Each span is 1000 cm long and is equally divided into 20 segments for finite element analysis. A 20 KN concentrated load is applied upward to node 27. Damage is imposed to element 13 with damage indices equal to 0.2, 0.4, 0.6, and 0.8, respectively. Since the infected damage location is on the left hand side of the span, we shall focus numerical variations only on this part.

Table 2 lists the calculated stresses and strains of the intact structure. Similar results can be obtained for all the other damage cases. Fig. 4 shows the distribution of bending, shearing, and

Table 2 Stress and strain fields of the intact structure

elem. No.	curvature	shear strain	shear force	rotation	translation	moment
1	6.32E-07	-8.59E-05	-1.75E+04	-4.20E-03	-1.05E-01	4.37E+05
2	1.90E-06	-8.59E-05	-1.75E+04	-4.13E-03	-3.14E-01	1.31E+06
3	3.16E-06	-8.59E-05	-1.75E+04	-4.01E-03	-5.17E-01	2.19E+06
4	4.42E-06	-8.59E-05	-1.75E+04	-3.82E-03	-7.13E-01	3.06E+06
5	5.69E-06	-8.59E-05	-1.75E+04	-3.57E-03	-8.98E-01	3.94E+06
6	6.95E-06	-8.59E-05	-1.75E+04	-3.25E-03	-1.07E+00	4.81E+06
7	8.21E-06	-8.59E-05	-1.75E+04	-2.87E-03	-1.22E+00	5.69E+06
8	9.48E-06	-8.59E-05	-1.75E+04	-2.43E-03	-1.35E+00	6.56E+06
9	1.07E-05	-8.59E-05	-1.75E+04	-1.92E-03	-1.46E+00	7.43E+06
10	1.20E-05	-8.59E-05	-1.75E+04	-1.35E-03	-1.55E+00	8.31E+06
11	1.33E-05	-8.59E-05	-1.75E+04	-7.21E-04	-1.60E+00	9.18E+06
12	1.45E-05	-8.59E-05	-1.75E+04	-2.64E-05	-1.62E+00	1.01E+07
13	1.58E-05	-8.59E-05	-1.75E+04	7.32E-04	-1.60E+00	1.09E+07
14	1.71E-05	-8.59E-05	-1.75E+04	1.55E-03	-1.54E+00	1.18E+07
15	1.83E-05	-8.59E-05	-1.75E+04	2.44E-03	-1.44E+00	1.27E+07
16	1.96E-05	-8.59E-05	-1.75E+04	3.39E-03	-1.30E+00	1.36E+07
17	2.09E-05	-8.59E-05	-1.75E+04	4.40E-03	-1.10E+00	1.44E+07
18	2.21E-05	-8.59E-05	-1.75E+04	5.47E-03	-8.57E-01	1.53E+07
19	2.34E-05	-8.59E-05	-1.75E+04	6.61E-03	-5.55E-01	1.62E+07
20	2.46E-05	-8.59E-05	-1.75E+04	7.81E-03	-1.95E-01	1.71E+07

rotation energy quantities along the bridge girder. The individual quantity on an element is not the same but their summation becomes a constant for the intact structure as expected. Once structural deficiencies occur, *P* energy will no longer be a constant across the damage location as shown in Fig. 5. Considering that damage locations are the unknown to be found in real life. They are omitted intentionally from the plotting for the time being. Then the SDE diagram from the first implementation can be shown as in Fig. 6. The ratios are ranged approximately from 16 to 18.5 in this case. It appears to be exactly the proposed pattern: two different energy constants are separated by a sharp vertical drop right at the damaged location.

From the second implementation method, incremental quantities of the stress and strain fields are used. The variation energy components along the bridge are not constantly distributed as shown in Fig. 7. Nevertheless, summation from the contribution terms remains constant for intact structure and two different quantities for damaged structure as shown in Fig. 8. Both methods successfully provide the damage information.

Case 2. A continuous steel bridge-2

We shall examine the effect of SDE under different loading position in this case. All the condition is the same as in case 1 except that the load application point has been moved from node 27 to 32. Although the displacement shapes and distributed strain pattern are found to be quite similar to those in case 1, they are not equal numerically. The pattern of SDE diagrams from both implementation methods are the same as shown in Fig. 9. They are not affected by the loading
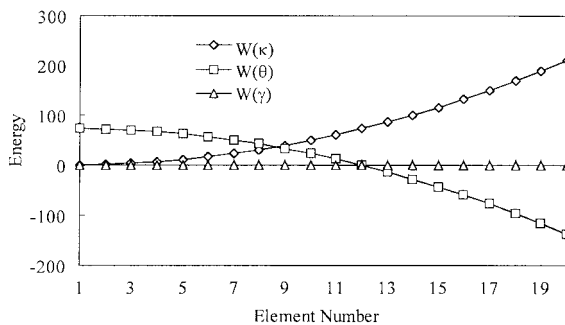

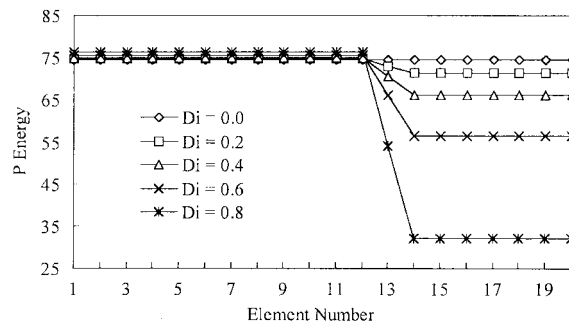Fig. 4 Energy distribution of an intact span

Fig. 5 *P* energy for different damage indices
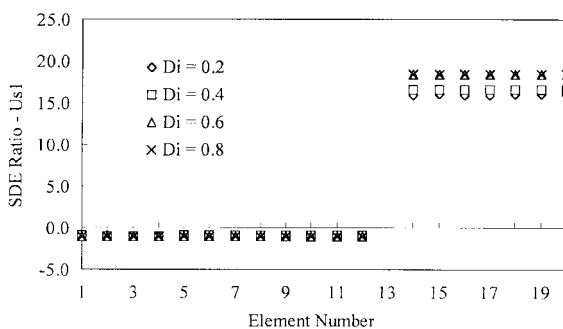

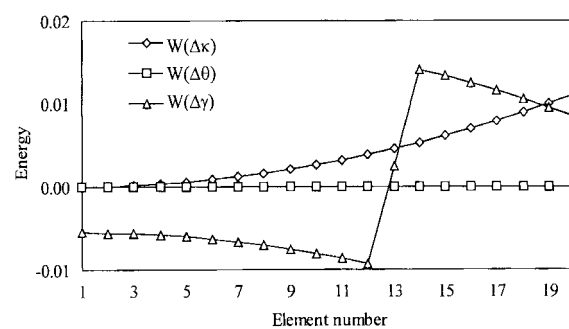Fig. 6 SDE ratio from the first implementation

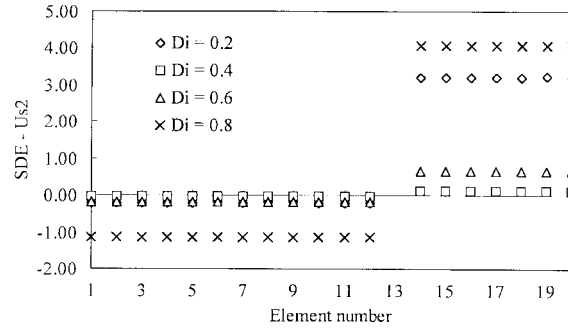Fig. 7 Variation of the energy components for

Fig. 8 SDE from the second implementation

positions.

Case 3. An aluminum bridge

We shall examine the effect of loading type to SDE in this case. We use exactly the same dimensions, cross-section, and the FEM model as it was in the previous cases except that steel material has been replaced by aluminum. In addition, a 500 N/m uniformly distributed load is imposed downward throughout the right-hand-side of the span. It creates negative displacement which is different from the previous cases to the damaged area. The absolute maximum displacement at the damaged element is much smaller than that in case No. 1. But no matter how
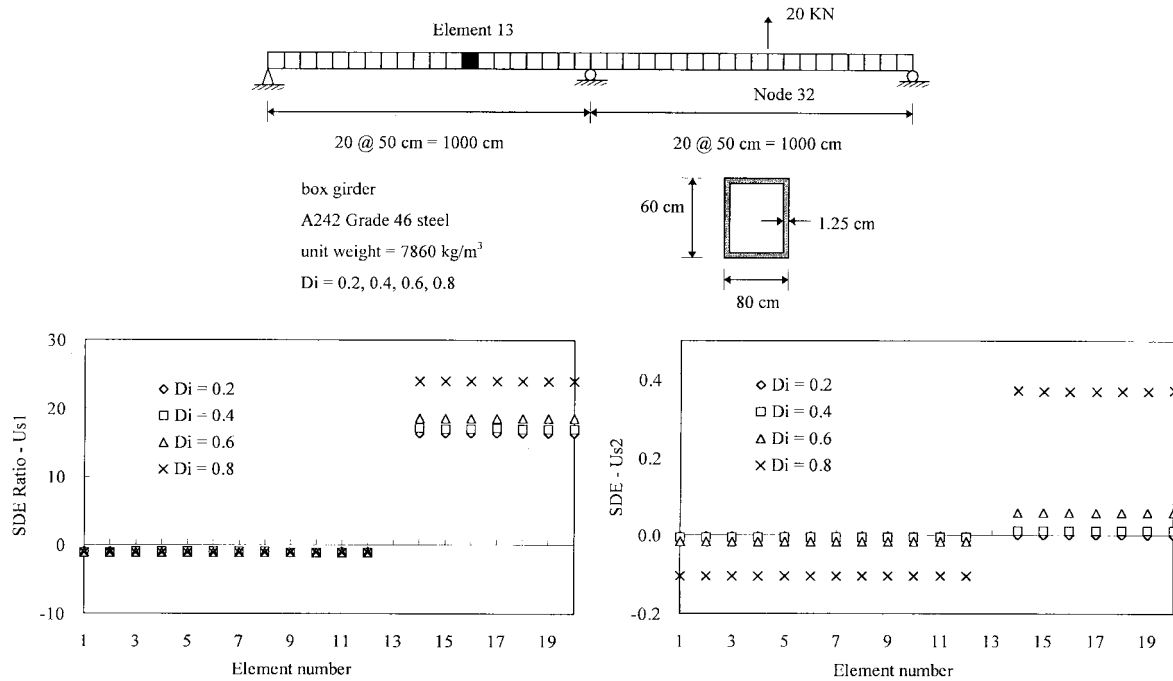

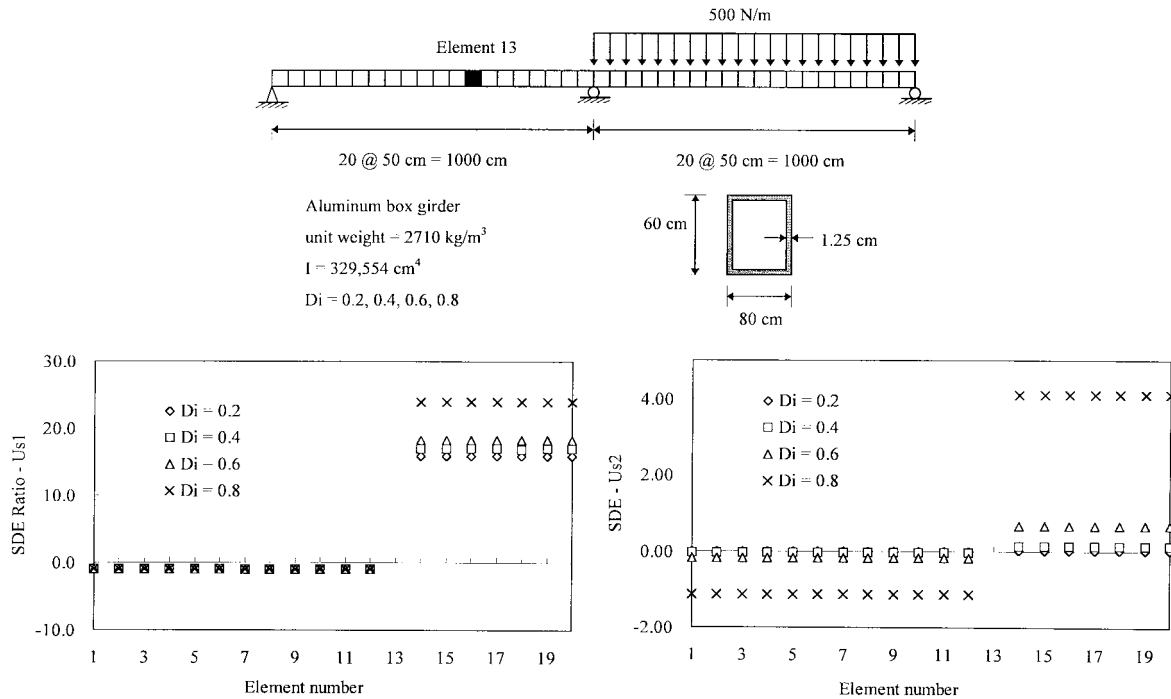Fig. 9 SDE of the steel continuous girder for Case 2

Fig. 10 SDE of the aluminum girder under distributed load

small it is, the defect energy parameter performs successfully as long as the displacement and strain quantities are differentiable. Results for both *Us*1 and *Us*2 are successful and equally good as shown in Fig. 10. As compared to the previous cases, it provides the evidence that the SDE are not affected by the loading patterns nor the materials.

Case 4. A non-prismatic cantilever beam

Structural constraints and cross-sections are changed in this case. A non-prismatic cantilever beam is composed of two steel rods: one is 10 cm, the other is 20 cm in their radii. A 500N concentrated load is applied at the free end. The SDE diagrams are plotted in Fig. 11. Obvious vertical drops occur at the damaged location. It is interesting to find that, in this special case, there is no energy change occurring at the junction of the two cross-sections. However, this is not always the case. In the other non-prismatic beam examples, small and yet significant vertical drops might occur. The stress fields are continuous across the intersection but the strains are not. Since SDE is partially contributed from strains, it is natural to create a gap at the intersection of the members. Fortunately, this location is always known. Special attention should always be paid to the particular structural junction whenever a safety inspection is made.

Variations of the stresses and strains between the fixed end and the damage location are found to be very tiny. It causes the SDE very close to zero for both implementation methods for each damage index. This is unique for cantilever beams.
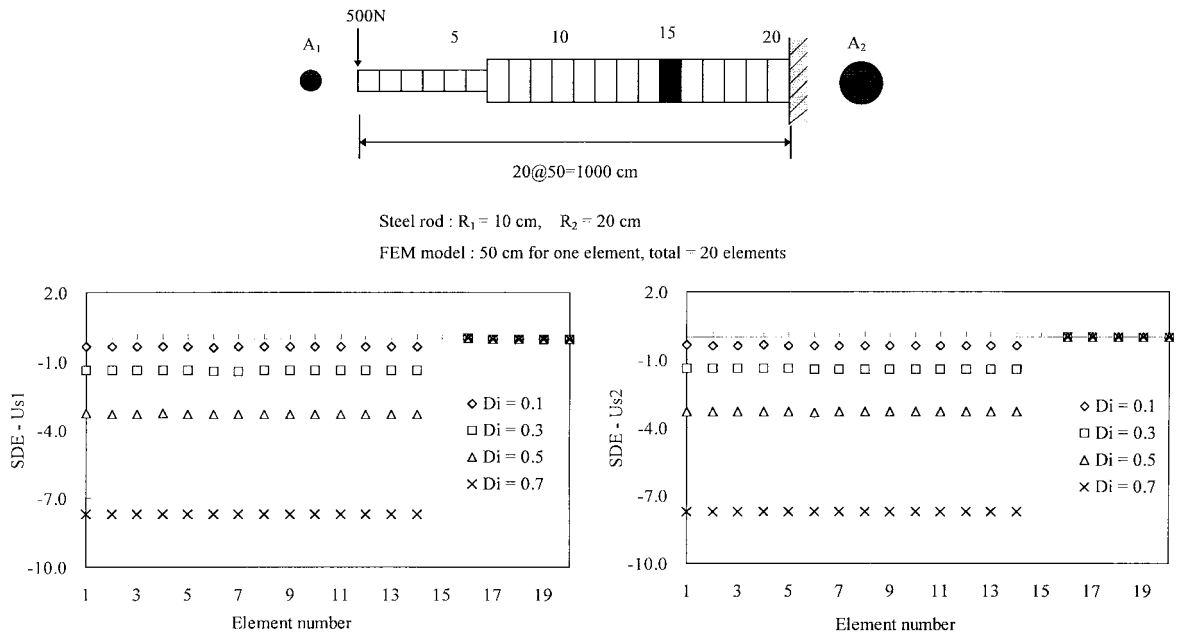
Fig. 11 SDE of the non-prismatic cantilever beam for Case 4

Case 5. A light gage cold-form section

Lightweight structure has become one of the major structural types in sports, leisure and entertainment facilities. It provides the following advantages in material aspect as well as in building construction: high strength-to-weight ratios, mass production and easy prefabrication, fast erection and installation, non-shrinking and non-creeping at ambient temperatures. Its unusual cross-sections designed for any specific purpose can be economically produced by cold-forming operations. Therefore, its application to large-scale civil structures has become more and more frequently used and important.

A 450 cm long simply supported girder is divided into 90 elements. Its cross-section is made of two "*Cs*" connected back to back. We intend to investigate not only the performance of lightweight section but also the sensitivity of SDE to a localized damage. One out of 90 elements with damage index equals 0.01, 0.05, 0.1 and 0.2, respectively, can really capture the sense of a localized damage. Calculation results show that for 1% damage, SDE were somewhat diverse. However, damage patterns still can be recognized. As damage severity increases, SDE diagram converges as shown in Fig. 12. Theoretically, any slight change in material constants will be reflected in the SDE diagram. Divergence was resulted from the truncated errors in numerical calculations especially dealing with such tiny change.

Vertical drop occurs on element 60 were caused by the loading effect. Concentrated loads including internal support reactions are not counted between the evaluation points unless a modification formula is applied. Let F be the concentrated force, a $F\theta$ term can be added to the P scalar to eliminate concentrated load effect if desired. Actually, the modification process is not recommended because location of the load application point is always known.

In Fig. 13, SDE for the second implementation is shown. Height of the energy rise is proportional
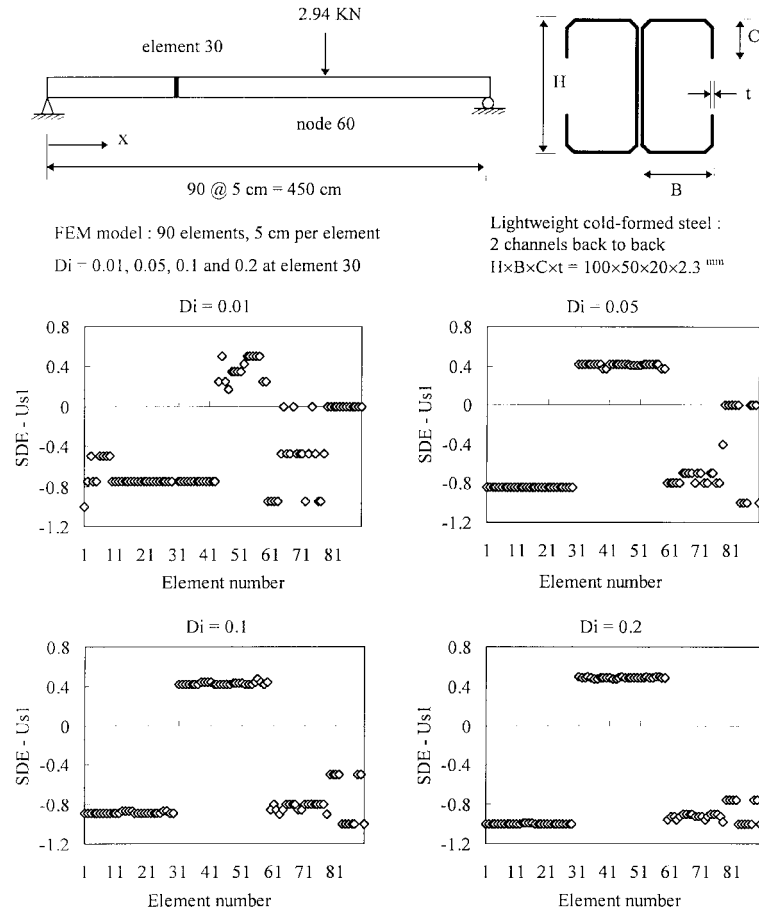
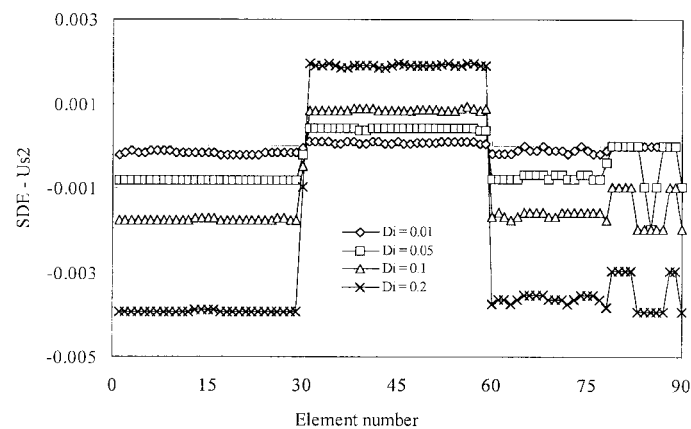Fig. 12 SDE of the light gage cold-form steel from the first implementation

Fig. 13 SDE of the light gage cold-form steel from the second implementation
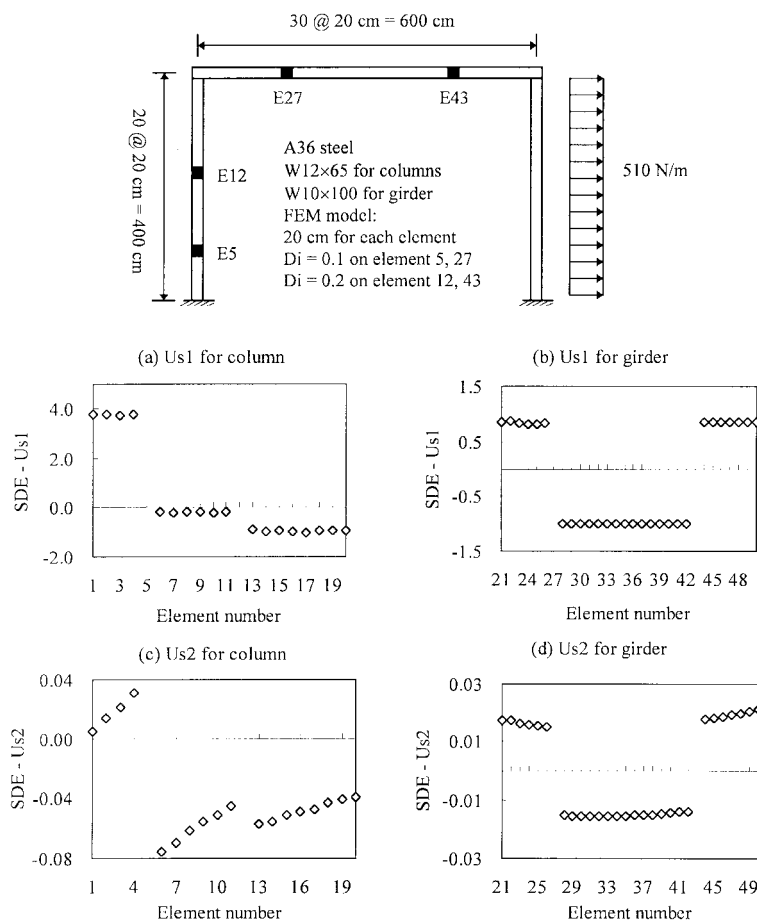
Fig. 14 SDE diagram of the rigid frame for Case 6

to the damage indices.

Case 6. A rigid frame

A portal frame is designed to transfer horizontal uniform forces caused by wind, earthquake, and traffic loading to its fixed supports. W12 × 65 and W10 × 100 shapes from AISC manual were selected as the columns and girder, respectively. Dimensions, properties and the finite element model of the rigid frame are shown in Fig. 14. Multiple damage condition is introduced to girder and column. On element 5 and 27, $Di = 0.1$; while on element 12 and 43, $Di = 0.2$. In this case, height of the vertical step does not in proportion to damage index but the existence and location of damage are detected for both girder and column.

4. Conclusions

From numerical simulation results, the following conclusions about static defect energy parameter

and its applications can be drawn:

(1) Static load can be applied at any convenient location. All the results are successful and equally good.
(2) Both concentrated and uniformly distributed loads are acceptable.
(3) No matter how small the stresses and strains are, SDE performs successfully as long as they are differentiable.
(4) The SDE can be applied to both prismatic and non-prismatic members.
(5) It is also applicable to any homogeneous and isotropic material, of different cross sections, and to beam and frame structures under different boundary conditions.
(6) The SDE is also applicable for multiple damage detection.
(7) This parameter is very sensitive to reflect localized damage.
(8) Although there is no numerical relationship that can be found at this moment, there is a tendency that severe damage will create higher energy gap.

Acknowledgements

References

Banan, M.R. and Hjelmstad, K.D. (1994), "Parameter estimation of structures from static responses, I: Computational aspects", *ASCE J. Stru. Eng.*, **120**(11), 3243-3258.

Banan, M.R. and Hjelmstad, K.D., "Parameter estimation of structures from static responses, II: Numerical simulation studies", *ASCE J. Stru. Eng.*, **120**(11), 3259-3283.

Christides, S. and Barr, A.D.S. (1984), "One-dimensional theory of cracked Bernaulli-Euler beams", *Int. J. Mech. Sci.*, **26**(11/12), 639-648.

Christides, S. and Barr, A.D.S. (1986), "Torsional vibration of cracked beam of non-circular cross section", *Int. J. Mech. Sci.*, **28**(7), 473-490.

Gudmundson, P. (1982), "Eigenfrequency changes of structures due to crack, notches or other geometrical changes", *J. Mech. and Physics of Solids*, **30**(5), 339-352.

Gudmundson, P. (1983), "The dynamic behavior of slender structures with cross section cracks", *J. Mech. and Physics of Solids*, **31**(4), 329-345.

Hajela, P. and Soeiro, F.J. (1990), "Structural damage detection based on static and modal analysis", *AIAA J.*, **28**(6), 1110-1115.

Sanayei, M. and Onipede, O. (1991), "Damage assessment of structures using static test data", *AIAA J.*, **29**(7), 1174-1179.

Notations

A	intact cross-section area
A_d	damaged cross-section area
B	basic force matrix
b	damaged depth of an element
c	$\cos \alpha$

Di	damage index
$\boldsymbol{D}_s$	specified deformation matrix
$\boldsymbol{D}_u$	unknown deformation matrix
$\boldsymbol{d}$	element end deformation matrix in global coordinate
$\boldsymbol{d}'$	element end deformation matrix in local coordinate
E	Young's modulus
F	concentrated force vector
$\boldsymbol{F}_s$	unknown force matrix
$\boldsymbol{F}_u$	specified force matrix
$\boldsymbol{f}$	element end force matrix in global coordinate
$\boldsymbol{f}'$	element end force matrix in local coordinate
G	shear modulus
$\boldsymbol{H}$	link matrix of the equilibrium equation
h	depth of an element
I	second moment of inertia
$\boldsymbol{K}$	unconstrained structural stiffness matrix
$\boldsymbol{K}_{uu}, \boldsymbol{K}_{us}, \boldsymbol{K}_{su}, \boldsymbol{K}_{ss}$ subdivided matrices of $\boldsymbol{K}$	
$\underline{\boldsymbol{k}}$	element global stiffness matrix
$\bar{\boldsymbol{k}}$	element basic stiffness matrix
$\boldsymbol{k}'$	element local stiffness matrix
M_i, M_j	element end moment corresponding to node i and j
N	axial force
N_e	number of element
$\boldsymbol{R}$	rotation matrix
s	$\sin \alpha$
T	superscript, transformation of a matrix
V	shear force
Δ	basic deformation matrix
δ	elongation of an element
θ_i, θ_j	element rotation corresponding to node i and j
α	elements orientation angle
ε	axial elongation
κ	curvature
γ	shear strain
γ_c	shear correction factor